Journal of Sound and Vibration 438 (2019) 83–98

Contents lists available at ScienceDirect

Journal of Sound and Vibration

journal homepage: www.elsevier.com/locate/jsvi

Frequency response and resonance of a thin fluid film bounded by elastic sheets with application to mechanical filters

Arie Tulchinsky, Amir D. Gat *

Faculty of Mechanical Engineering, Technion - Israel Institute of Technology, Haifa 3200003, Israel

ARTICLE INFO

Article history:
Received 8 February 2018
Revised 4 July 2018
Accepted 22 August 2018
Available online 7 September 2018
Handling Editor: D. Juve

Keywords:
Vibrations
Layered structure

ABSTRACT

We study steady-state oscillations of a thin viscous film bounded by two elastic sheets, excited by traveling pressure waves over its upper surface. The fluid within the cell is bounded by two asymmetric elastic sheets which are connected to a rigid surface via distributed springs. The fluid is modeled by the unsteady thin film lubrication approximation and the sheets are modeled by the linearized plate theory. Modal analysis yields the frequency response of the configuration as a function of three parameters: the fluidic Womersley number and the ratio of solid stress to viscous pressure for each of the sheets. These ratios, analogous to the Capillary number, combine the effects of fluid viscosity and the sheets inertia, bending and tension. The resonance frequencies of the configuration include the resonance frequency of the upper sheet, the resonance frequency of both sheets, and a new resonance frequency related to the interaction between the fluidic motion parallel to the elastic solids and the relative elastic displacements. Near the resonance frequency of the upper sheet, the fluid pressure is identical in amplitude and phase to the external excitation. For configurations where both sheets are near resonance, small changes in frequency yield significant modification of the fluidic pressure. The amplitude ratio of the fluidic pressure to the external pressure is presented vs. frequency for several characteristic solid and fluid properties, yielding a bandpass filter behaviour. The results presented here suggest fluid embedded structures may be utilized as protective surfaces and mechanical filters.

1. Introduction

In this work we examine the frequency response of two parallel elastic sheets containing a thin liquid film. We focus on physical regimes where viscous, elastic and inertial effects (of the fluid and solids) are of similar order of magnitude. The elastic sheets are modeled by the linear plate theory and include both bending and tension effects, and may be connected to a rigid surface via distributed springs.

Interaction of fluid viscosity with solid elasticity in geometries involving viscous film bounded by two parallel elastic plates (commonly known as Hele-Shaw cells), or similar configurations, is relevant to various research subjects. Among these are viscous peeling problems [1–5], fluid-driven crack propagation [6–8], gravity currents spreading under elastic sheets [9,10], and wrinkling of lubricated sheets [11,12]. At the inviscid flow limit, elastic-inertial fluid-structure-interaction have been shown to vary the solid structure resonance frequency. Initial work on the subject was pioneered by H. Lamb [13] who examined the modified resonance frequencies of a clamped plate in contact with a water reservoir. This work has been extended by various

* Corresponding author.
E-mail address: amirgat@technion.ac.il (A.D. Gat).

https://doi.org/10.1016/j.jsv.2018.08.047
0022-460X/

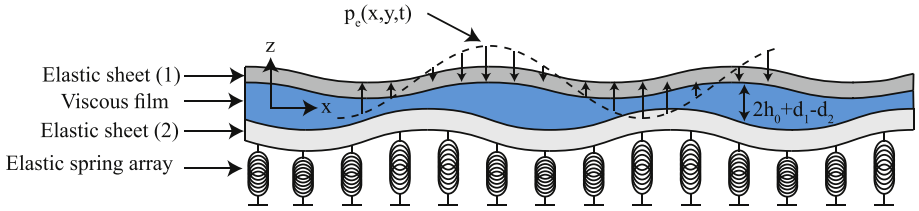

Fig. 1. Illustration of the configuration and the Cartesian coordinate system. Both elastic sheets are parallel at rest to the $x-y$ plane. $p_e(x,y,t)$ is the external propagating pressure wave, $2h_0$ is the gap between the sheets at rest, d_1 and d_2 are the displacements of plate 1 and 2 in the z-direction, respectively.

researchers including [14–16]. Recent works on the dynamic response of elastic sheets interacting with inviscid laminar flows include [17–19].

Various previous studies examined leveraging fluidic elements, contained within a solid structure, to increase structural rigidity and damping of external loads. Commonly used mechanisms include the tuned liquid column dampers (TLCD) [20,21] and viscous damping devices (VDD), which were studied extensively [22,23]. Other approaches include utilizing shear-thickening-fluids as a mechanism to improve shock-absorption for body armor applications [24–26], as well as combining a lyophobic fluid with a porous matrix to create colloidal suspensions [27]. The current work follows the approach of our previous study [28], examining an elastic Hele-Shaw configuration as a structural element. In Ref. [28], we studied the transient dynamics of elastic Hele-Shaw Cells due to localized excitations, assuming rigid lower surface and neglecting elastic tension effects and inertia in both the solid and fluid.

We here examine the frequency response of steady-state oscillations of two elastic plates containing a viscous film and include inertial effects of both the fluid and solid regions. Specifically, we aim to obtain extrema of fluidic pressure and solid displacements in terms of the excitation frequency and the mechanical properties of the system. The results of the current research allow to compute, via Fourier transform, the effect of an internal viscous film on the response of elastic sheets to a general external loading. This, in turn, enables optimizing the design of such solid-liquid configurations as protective layers, via maximizing resistance to external shocks and oscillations. The structure of this paper is as follows: In section 2 we define and scale the problem. In section 3 we obtain the phase and amplitude of traveling-wave solutions. In section 4 we present a comprehensive parametric study of frequency response in terms of solid displacements and fluidic pressure for various configurations. In section 5 we summarize and discuss the results presented in section 4, examine new resonance frequency related to fluid motion parallel to the sheets (section 5.1), and illustrate realization of Hele-Shaw cells as mechanical filters or protective surfaces (section 5.2). In section 6 we provide concluding remarks.

2. Problem formulation and scaling

We study steady-state oscillations of two parallel elastic sheets containing a thin liquid film. The fluid flow and solid displacements are excited by an external pressure wave with prescribed frequency and wavelength, which may be readily generalized to an arbitrary external forcing. The elastic sheets are modeled by the linear plate theory and include bending, tension, and inertial effects.

The configuration and the Cartesian coordinate system $(\boldsymbol{x}_{\parallel}, z)$ are defined in Fig. 1, $\parallel$ subscript denotes two-dimensional vectors in the $x-y$ plane. The $x-y$ plane is parallel and of equal distance to both plates at rest. The subscripts 1 and 2 denote the upper and lower plates, respectively.

The fluidic properties are denoted by:

	p,	fluidic pressure,
	$(\boldsymbol{u}_{\parallel}, w)$,	fluid velocity,
	ρ,	fluid density,
and	μ,	fluidic dynamic viscosity.

The geometric and physical properties of the elastic sheets are given by (where $n = 1, 2$ denote the upper and lower sheet respectively):

	$2h_0$,	the gap between the plates at rest,
	s_k,	spring array stiffness,
	s_n,	elastic sheet bending stiffness,
	t_n,	sheet tension,
	b_n,	sheet thickness,
	m_n,	sheet mass-per-area,
and	$(\boldsymbol{d}_{\parallel,n}, d_n)$,	sheet displacement.

We assume an incompressible flow-field, corresponding to the limit of negligible fluidic volume changes due to pressure, compared with pressure-driven volume changes of the elastic boundaries. From scaling considerations, this limit is given by the relation

$$p\beta \ll \frac{d'^*}{h_0} \quad \text{or equivalently} \quad \beta \ll \frac{1}{k^4 h_0 s_n}, \frac{1}{k^2 h_0 t_n} \tag{1}$$

where $\beta = -1/\mathrm{V}(\partial V/\partial p)$ is fluidic compressibility, V is a given fluidic volume, d'^* is boundary deformation, and k is wavenumber. The dynamics of the Newtonian, incompressible fluid is governed by the Navier-Stokes equation

$$\rho\left[\frac{\partial}{\partial t} + (\boldsymbol{u}_\parallel, w)\cdot\left(\boldsymbol{\nabla}_\parallel, \frac{\partial}{\partial z}\right)\right](\boldsymbol{u}_\parallel, w) = -\left(\boldsymbol{\nabla}_\parallel, \frac{\partial}{\partial z}\right)p + \mu\left(\boldsymbol{\nabla}_\parallel, \frac{\partial}{\partial z}\right)^2(\boldsymbol{u}_\parallel, w), \tag{2}$$

and the continuity equation

$$\left(\boldsymbol{\nabla}_\parallel, \frac{\partial}{\partial z}\right)\cdot(\boldsymbol{u}_\parallel, w) = 0, \tag{3}$$

supplemented by no-slip and no-penetration at the fluid-solid interfaces

$$(\boldsymbol{u}_\parallel, w) = \left(\frac{\partial \boldsymbol{d}_{\parallel,1}}{\partial t} - \frac{b_1}{2}\boldsymbol{\nabla}_\parallel\frac{\partial d_1}{\partial t}, \frac{\partial d_1}{\partial t}\right), \quad z = h_0 + d_1 \tag{4a}$$

$$(\boldsymbol{u}_\parallel, w) = \left(\frac{\partial \boldsymbol{d}_{\parallel,2}}{\partial t} + \frac{b_2}{2}\boldsymbol{\nabla}_\parallel\frac{\partial d_2}{\partial t}, \frac{\partial d_2}{\partial t}\right), \quad z = -h_0 + d_2, \tag{4b}$$

consistent with the Kirchhoff hypothesis of linear displacements (d_1, d_2) with regard to the z-direction. The sheet deflections are governed by the linearized plate theory [29].

$$-s_1\nabla_\parallel^4 d_1 + t_1\nabla_\parallel^2 d_1 + p - p_e = m_1\frac{\partial^2 d_1}{\partial t^2}, \quad z = h_0 + d_1 \tag{5a}$$

$$-s_2\nabla_\parallel^4 d_2 + t_2\nabla_\parallel^2 d_2 - s_k d_2 - p = m_2\frac{\partial^2 d_2}{\partial t^2}, \quad z = -h_0 + d_2, \tag{5b}$$

where t_1, t_2 are considered uniform and isotropic. (The boundary conditions (5) may be reduced to a free surface description by setting $t_1 = \gamma$, and $s_1 = m_1 = 0$, where γ is surface tension.)

The external propagating pressure wave is the real part of the function

$$p_e = \widehat{p}_e e^{i(\boldsymbol{k}\cdot\boldsymbol{x}_\parallel + \omega t)} \tag{6}$$

where $\widehat{p}_e$ is the amplitude of the wave, $\boldsymbol{k}_\parallel$ is the wave vector, $k = |\sqrt{\boldsymbol{k}_\parallel\cdot\boldsymbol{k}_\parallel}|$ is the wavenumber, and ω is the angular frequency $(\widehat{p}_e, k, \omega \in \mathbb{R})$. For the purpose of separating the flow problem from the bulk deformation of the structure, we denote hereafter the deformation of the sheets by the average deformation

$$\overline{d} = \frac{d_1 + d_2}{2} \tag{7}$$

and relative deformation

$$d' = \frac{d_1 - d_2}{2}. \tag{8}$$

We define w' as

$$w' = w - \frac{\partial \overline{d}}{\partial t}, \tag{9}$$

where $\partial\overline{d}/\partial t$ represents fluid speed due to the mean motion of both sheets and w' is thus fluid speed due to the relative motion of the sheets.

Next we turn to scaling and order-of-magnitude analysis. Hereafter, asterisk superscripts denote characteristic values and Capital letters denote normalized variables. The characteristic $\boldsymbol{x}_\parallel$ plane fluid velocity is u^*, the characteristic z-direction fluid velocity is w'^*, the characteristic fluid pressure is p^*, the characteristic mean deformation is $\overline{d}^*$ and the characteristic relative deformation is d'^*.

We define the following small parameters

$$\varepsilon_1 = h_0 k \ll 1, \quad \varepsilon_2 = \frac{d'^*}{h_0} \ll 1 \tag{10}$$

corresponding to requirements of slender configuration and small relative deformation to fluid gap height. We define normalized coordinates $(\boldsymbol{X}_{\parallel}, Z)$ and time T

$$(\boldsymbol{X}_{\parallel}, Z) = \left(\boldsymbol{x}_{\parallel} k, \frac{z}{h_0}\right), \quad T = t\omega, \tag{11a}$$

normalized mean $\overline{D}$ and relative D' sheet deflections

$$\overline{D} = \frac{\overline{d}}{\overline{d}^*}, \quad D' = \frac{d'}{d'^*} \tag{11b}$$

normalized fluid velocity

$$\boldsymbol{U}_{\parallel} = \frac{\boldsymbol{u}_{\parallel}}{u^*}, \quad \overline{W} = \frac{\overline{w}}{\omega \overline{d}^*}, \quad \overline{W}' = \frac{\overline{w}'}{\omega d'^*} \tag{11c}$$

and normalized fluid pressure P and external pressure P_e

$$P = \frac{p}{p^*}, \quad P_e = \frac{p_e}{p^*}. \tag{11d}$$

Substituting (11) into (2) and (3) yields the leading order momentum equations

$$\alpha^2 \frac{\partial \boldsymbol{U}_{\parallel}}{\partial T} = -\boldsymbol{\nabla} P + \frac{\partial^2 \boldsymbol{U}_{\parallel}}{\partial Z^2} + O\left(\varepsilon_1^2, \varepsilon_1 \mathrm{Re}, \frac{\overline{d}^*}{d^{*\prime}} \varepsilon_1 \mathrm{Re}\right), \tag{12a}$$

$$\alpha^2 \varepsilon_1^2 \left(\frac{\partial^2 D'}{\partial T^2} + \frac{\overline{d}^*}{d^{*\prime}} \frac{\partial^2 \overline{D}}{\partial T^2}\right) = -\frac{\partial P}{\partial Z} + O\left(\varepsilon_1^2, \varepsilon_1^3 \mathrm{Re}, \frac{\overline{d}^*}{d^{*\prime}} \varepsilon_1^3 \mathrm{Re}\right), \tag{12b}$$

and continuity equation

$$\frac{\partial W'}{\partial Z} + \boldsymbol{\nabla} \cdot \boldsymbol{U}_{\parallel} = 0, \tag{12c}$$

where $\mathrm{Re} = \rho_l h_0 u^* / \mu$ is the Reynolds number and $\alpha^2 = \rho_l h_0^2 \omega / \mu$ is the Womersley number.

Order of magnitude analysis of (12) yields $d'^* \omega / u^* \sim \varepsilon_1$, $p^* h_0^2 k / \mu u^* \sim 1$, and $\varepsilon_1 \mathrm{Re} / \alpha^2 = \varepsilon_2$. Since the linear time-derivative inertial term $\partial(\boldsymbol{u}_{\parallel}, w)/\partial t$ in the LHS of (2) scales with α^2 while the non-linear convective terms $(\boldsymbol{u}_{\parallel}, w) \cdot (\boldsymbol{\nabla}, \partial/\partial z)(\boldsymbol{u}_{\parallel}, w)$ scale with $\varepsilon_1 \mathrm{Re} = \alpha^2 \varepsilon_2$, we obtain the linearized Navier-Stokes momentum equations without any further assumptions. In addition, from $\varepsilon_2 \ll 1$ we obtain a restriction on the phase velocity of the wave $\omega/k \gg u^*$.

We substitute (11) into (4) and (5) to obtain the leading order boundary conditions

$$W'(Z \sim 1) = \frac{\partial D'}{\partial T} + O(\varepsilon_2), \quad \boldsymbol{U}_{\parallel}(Z \sim 1) = O\left(b_1 k \varepsilon_1, \frac{\varepsilon_1^5 p^{*2} k}{2\mu\omega}\right), \tag{13a}$$

$$W'(Z \sim -1) = -\frac{\partial D'}{\partial T} + O(\varepsilon_2), \quad \boldsymbol{U}_{\parallel}(Z \sim -1) = O\left(b_2 k \varepsilon_1, \frac{\varepsilon_1^5 p^{*2} k}{2\mu\omega}\right), \tag{13b}$$

$$\left(\frac{-s_1 k^6 h_0^3}{\mu\omega} \nabla_{\parallel}^4 + \frac{t_1 k^4 h_0^3}{\mu\omega} \nabla_{\parallel}^2 - \frac{m_1 \omega h_0^3 k^2}{\mu} \frac{\partial^2}{\partial T^2}\right)\left(\overline{D} + D'\right) + P - P_e = 0 \tag{13c}$$

and

$$\left(-\frac{s_2 k^6 h_0^3}{\mu\omega} \nabla_{\parallel}^4 + \frac{t_2 k^4 h_0^3}{\mu\omega} \nabla_{\parallel}^2 - \frac{s_k h_0^3 k^2}{\mu\omega} - \frac{m_2 \omega h_0^3 k^2}{\mu} \frac{\partial^2}{\partial T^2}\right)\left(\overline{D} - D'\right) - P = 0. \tag{13d}$$

In (13c,d), $b_1 k, b_2 k \ll 1$ are necessary conditions for applying linear plate theory and $\varepsilon_1^5 p^{*2} k / 2\mu\omega \ll 1$ is a requirement of negligible effect of longitudinal displacements of the sheets on fluid velocity.

We focus hereafter on $\overline{d}^* \sim d'^*$ as well as $\alpha^2 = O(1)$. Thus, the order of magnitude of the sheet displacements are $d'^* \sim h_0^3 p^* k^2 / \mu\omega$ and the fluidic pressure due to transverse acceleration is negligible ($\partial P / \partial Z \sim 0$, see (12b)). Leading order governing equations, boundary conditions and order of magnitude for the case of dominant effect of transverse acceleration on fluidic pressure are presented in Appendix A.

3. Phase and amplitude of traveling-wave solutions

We study steady state oscillations, and thus examine traveling-wave solutions of frequency ω and wave vector $\boldsymbol{k}$ equal to the external excitation pressure wave. Without loss of generality, we focus on two-dimensional configurations where the wave vector is parallel to the x-direction. We thus seek solutions of the form

$$\begin{pmatrix} U \\ W \\ \overline{D} \\ D' \\ P \\ P_e \end{pmatrix} = \begin{pmatrix} \widehat{U}(Z) \\ \widehat{W}(Z) \\ \widehat{\overline{D}} \\ \widehat{D}' \\ \widehat{P} \\ \widehat{P}_e \end{pmatrix} e^{i(X+T)}. \tag{14}$$

The parameters with hat superscript (e.g. $\widehat{U}$) represent the complex amplitude of the wave-form solutions.

Substituting (14) into (12) and (13), we simplify the governing Eq. (12a-c)

$$\alpha^2 i\widehat{U} - \frac{\partial^2 \widehat{U}}{\partial Z^2} \sim -i\widehat{P}, \quad \frac{\partial \widehat{P}}{\partial Z} \sim 0, \quad \frac{\partial \widehat{W}'}{\partial Z} + i\widehat{U} = 0, \tag{15}$$

as well as the boundary conditions to (13)

$$\widehat{W}'(1) + \widehat{W}'(-1) \sim 0, \quad \widehat{W}'(1) - \widehat{W}'(-1) \sim 2i\widehat{D}', \quad \widehat{U}(1) \sim \widehat{U}(-1) \sim 0, \tag{16a}$$

and

$$Z_1\left(\widehat{\overline{D}} + \widehat{D}'\right) = \widehat{P}_e - \widehat{P}, \quad Z_2\left(\widehat{\overline{D}} - \widehat{D}'\right) = \widehat{P}, \tag{16b}$$

where the dimensionless parameters Z_1 and Z_2 are defined by ($n = 1, 2$)

$$Z_n = \frac{-s_n k^4 - t_n k^2 + m_n \omega^2 - s_k(n-1)}{\mu\omega / h_0^3 k^2} \tag{17}$$

which may be interpreted as the ratio between the inertial and elastic stress within the solid and the traction applied by the fluid due to the viscous squeeze flow. ($1/Z_n$ is analogous to the Capillary number for thin films, C_a.) The limits of $Z_1 \to 0$ and $Z_2 \to 0$ correspond to resonance of elastic sheets 1 and 2, respectively. Negative values of Z_1 and Z_2 are associated with dominant elastic bending and tension effects whereas positive values are associated with dominant inertial effects.

We initially solve ((15)) together with ((16a)) to obtain the longitudinal fluid velocity

$$\widehat{U} = \left(\frac{\cosh(\sqrt{\alpha^2 i}Z)}{\cosh(\sqrt{\alpha^2 i})} - 1\right)\frac{\widehat{P}}{\alpha^2}. \tag{18}$$

We substitute (18) into (15), integrate with respect to Z, and apply (16a) to obtain the transverse liquid velocity

$$\widehat{W}' = i\left(Z - \frac{\sinh(\sqrt{\alpha^2 i}Z)}{\sqrt{\alpha^2 i}\cosh(\sqrt{\alpha^2 i})}\right)\frac{\widehat{P}}{\alpha^2}. \tag{19}$$

Substituting into (16a) we obtain the relative sheet deflection

$$\widehat{D}' = \left(1 - \frac{\tanh(\sqrt{\alpha^2 i})}{\sqrt{\alpha^2 i}}\right)\frac{\widehat{P}}{\alpha^2}. \tag{20}$$

We substitute (20) into (16a) and obtain the mean sheet deformation

$$\widehat{\overline{D}} = \left(\frac{1}{\alpha^2}\left(1 - \frac{\tanh(\sqrt{\alpha^2 i})}{\sqrt{\alpha^2 i}}\right) + \frac{1}{Z_2}\right)\widehat{P}. \tag{21}$$

Finally, we subtract ((16b)) and substitute (20) to obtain the liquid pressure

$$\widehat{P} = \left(\frac{2Z_1}{\alpha^2}\left(1 - \frac{\tanh(\sqrt{\alpha^2 i})}{\sqrt{\alpha^2 i}}\right) + 1 + \frac{Z_1}{Z_2}\right)^{-1}\widehat{P}_e. \tag{22}$$

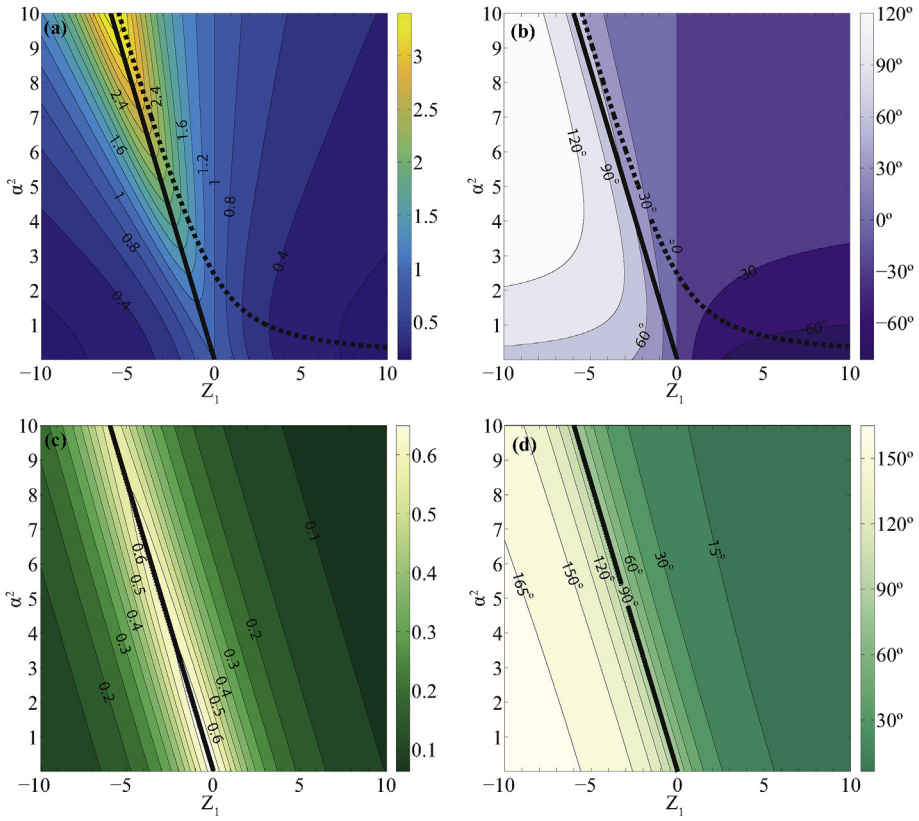

Fig. 2. Dynamics of a configuration with a lower rigid surface, i.e. $Z_2 \to \pm\infty$. (a) is the pressure ratio magnitude $|P/P_e|$, (b) is the phase between the liquid pressure and the external pressure $\angle P - \angle P_e$, (c) is the normalized magnitude of deformation $|D_1/P_e|$, and (d) is the phase of between the upper sheet deformation and the external pressure $\angle D_1 - \angle P_e$. The solid curve, defined by $\alpha^2 \sim -5Z_1/3$, indicates maximal magnitude of deformation and liquid pressure for constant α^2. The dashed curve indicates maximal magnitude of liquid pressure for constant Z_1 (this curve coincides with the solid curve in panels c,d).

We thus obtain $\widehat{U}, \widehat{W}', \widehat{D}', \widehat{\overline{D}}$ and $\widehat{P}$, representing the steady-state dynamics by a complex amplitude which is a function of the Womersley number α^2 and the sheets impedance Z_1 and Z_2. Solutions (18)–(22) in their dimensional form may be found in Appendix B, as well as the three-dimensional response dynamics for an arbitrary external pressure field.

For the limit of negligible fluidic inertial effects $\alpha^2 \to 0$ (18)–(22) may be further simplified. In this limit, the liquid pressure is

$$\widehat{P} \sim \left(1 + i\frac{2Z_1}{3} + \frac{Z_1}{Z_2}\right)^{-1} \widehat{P}_e, \tag{23}$$

the mean and relative deformations of the sheets are

$$\widehat{D}' \sim \frac{i\widehat{P}}{3}, \quad \widehat{\overline{D}} \sim \left(\frac{i}{3} + \frac{1}{Z_2}\right)\widehat{P} \tag{24}$$

and the fluid longitudinal and transverse speeds are

$$\widehat{U} \sim \frac{i(Z^2-1)\widehat{P}}{2}, \quad \widehat{W}' \sim \frac{(Z^3-3Z)\widehat{P}}{6}. \tag{25}$$

In the following section 4, a detailed parametric study of the results is presented in terms of the dimensionless parameters α^2, Z_1 and Z_2.

4. Maps and extrema lines of fluid pressure and elastic displacements

We here present and discuss the frequency response relations obtained in Section 3 and map (in Figs. 2–5) the amplitude and phase of liquid pressure and sheet deflection for various configurations. In all figures smooth lines represent values of Z_1 yielding extrema of the amplitude of the examined parameter for set values of (α^2, Z_2). Similarly, dotted lines represent values of α^2 yielding extrema points for set values of (Z_1, Z_2).

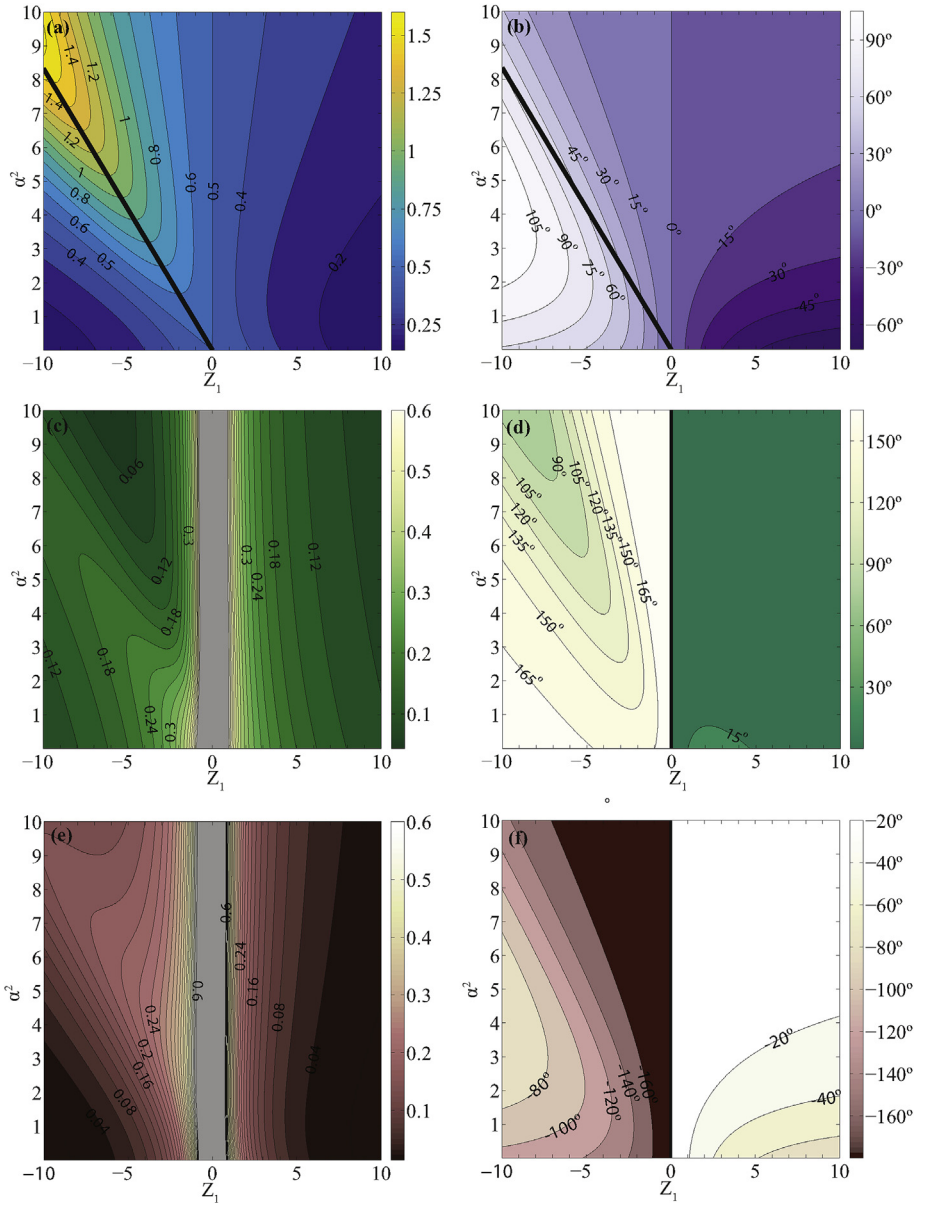

Fig. 3. Dynamics of a configuration consisting of two sheets with identical impedance, $Z_1 = Z_2$. Panel (a) shows $|P/P_e|$, panel (b) shows $\angle P - \angle P_e$, panel (c) shows $|D_1/P_e|$, panel (d) shows $\angle D_1 - \angle P_e$, panel (e) shows $|D_2/P_e|$, and panel (f) shows $\angle D_2 - \angle P_e$. Grey colored area indicates that the value of the variable exceeds the maximal value of the color bar and is singular at $Z_1 \sim 0$. The smooth line denotes values of Z_1 yielding extrema for predefined α^2. (For interpretation of the references to color in this figure legend, the reader is referred to the Web version of this article.)

Extrema of the fluidic pressure are readily obtained from (18)–(22), where for simplicity we seek extrema of $|P(\alpha^2, Z_1, Z_2)/P_e|$ by examining $|P_e/P|^2$, defined by

$$\left|\frac{P_e}{P}\right|^2 = \left(2Z_1F_1 + 1 + \frac{Z_1}{Z_2}\right)^2 + \left(2Z_1F_2\right)^2, \tag{26}$$

where

$$F_1(\alpha) = \frac{1}{\alpha^2} - \frac{2}{(2\alpha^2)^{\frac{3}{2}}}\left(\frac{\sinh\left(\sqrt{2\alpha^2}\right) + \sin\left(\sqrt{2\alpha^2}\right)}{\cosh\left(\sqrt{2\alpha^2}\right) + \cos\left(\sqrt{2\alpha^2}\right)}\right). \tag{27}$$

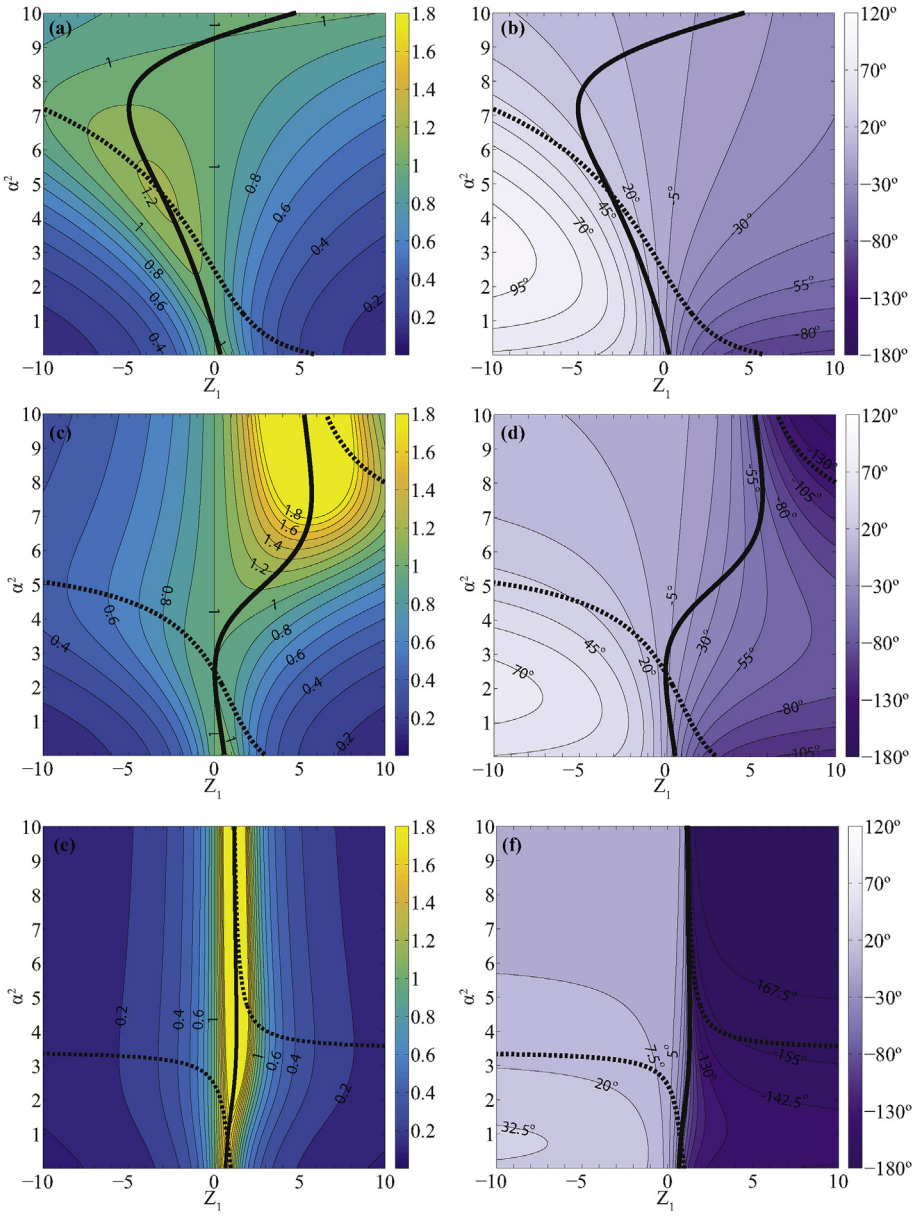

Fig. 4. Magnitude ratio and phase between the liquid pressure to external pressure as a function of α^2, and Z_1. The left column (a,c,e) shows $|\widehat{P}/\widehat{P}_e|$. The right column (b,d,f) shows $\angle\widehat{P} - \angle P_e$. Panels (a,b) present $Z_2 = -6$; panels (c,d) present $Z_2 = -3$, and panels (e,f) present $Z_2 = -1$. The smooth (29a) and dotted lines (29b) present extremum of deflection with regard to Z_1 (for set values of α^2, Z_2) and with regard to α^2 (for set values of Z_1, Z_2), respectively.

and

$$F_2(\alpha) = \frac{2}{(2\alpha^2)^{\frac{3}{2}}}\left(\frac{\sinh\left(\sqrt{2\alpha^2}\right) - \sin\left(\sqrt{2\alpha^2}\right)}{\cosh\left(\sqrt{2\alpha^2}\right) + \cos\left(\sqrt{2\alpha^2}\right)}\right). \tag{28}$$

By differentiation of Eq. (26) we obtain values of Z_1 yielding extrema of (26) for predefined (Z_2, α^2)

$$Z_1 = -\left(2F_1 + \frac{1}{Z_2}\right) \times \left[\left(2F_1 + \frac{1}{Z_2}\right)^2 + 4F_2^2\right]^{-1}. \tag{29a}$$

Similarly, values of Z_2 yielding extrema of (26) for predefined (Z_1, α^2) are

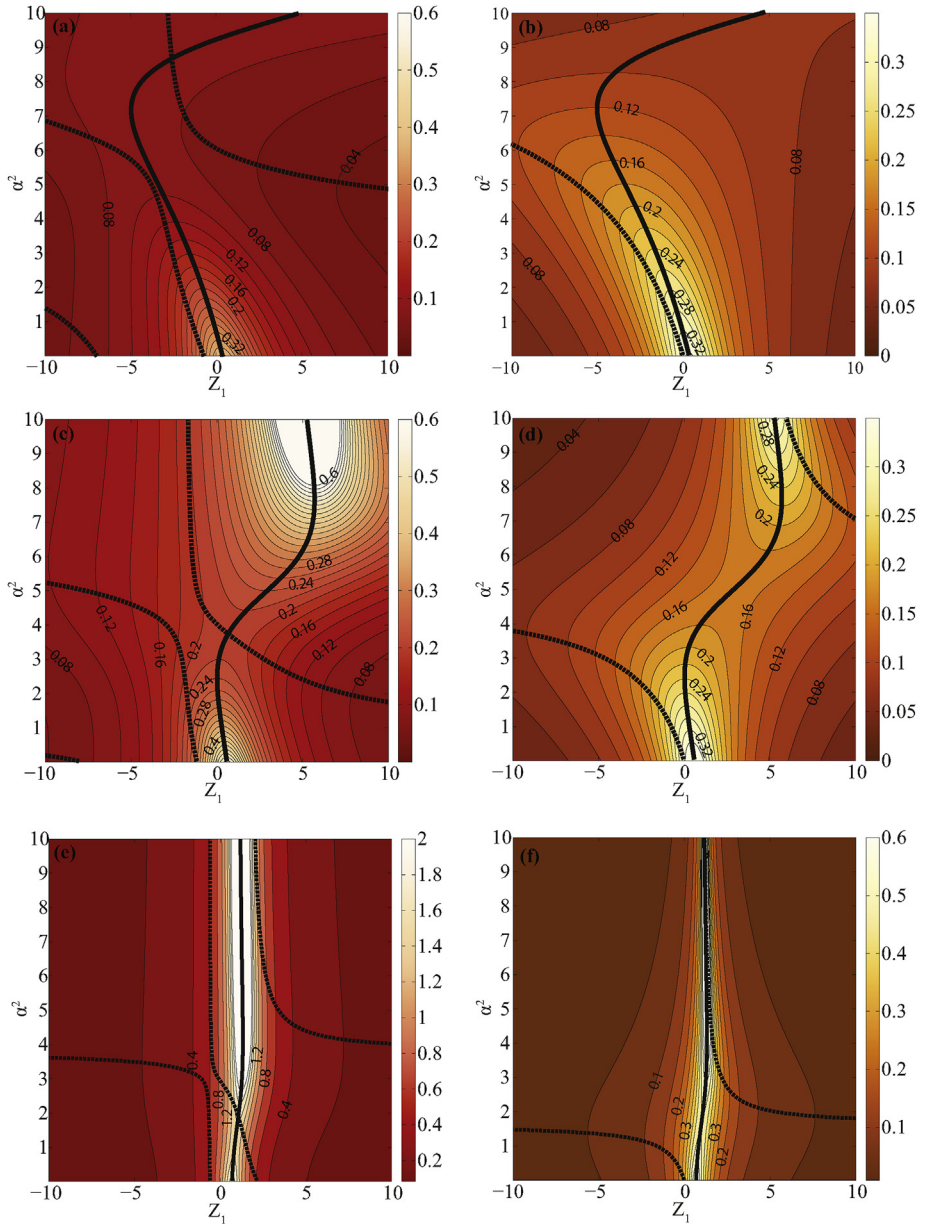

Fig. 5. Scaled average deformation magnitude $|\overline{D}|/|P_e|$ (a,c,e), and scaled relative deformation $|D'|/|P_e|$ (b,d,f), as a function of α^2, and Z_1. Panels (a,b) present $Z_2 = -6$; panels (c,d) present $Z_2 = -3$, and panels (e,f) present $Z_2 = -1$. The smooth and dotted lines present extremum of deflection with regard to Z_1 (for set values of α^2, Z_2) and with regard to α^2 (for set values of Z_1, Z_2), respectively (see Appendix C).

$$Z_2 = -\frac{Z_1}{2Z_1F_1 + 1}. \tag{29b}$$

Combining (29b) into (29a) yields the extrema $Z_1 = Z_2 = 0$ for a predefined value α^2, in which $|P(\alpha^2, Z_1, Z_2)/P_e|$ is singular and is determined by the limit of the ratio Z_1/Z_2.

Differentiating (26) with respect to α^2, an implicit relation for extrema in terms of α^2 for predefined values of both Z_1 and Z_2 is given by

$$Z_1\left[Z_1\frac{\partial}{\partial\alpha^2}\left(F_1^2 + F_2^2\right) + \frac{\partial F_1}{\partial\alpha^2}\left(1 + \frac{Z_1}{Z_2}\right)\right] = 0. \tag{29c}$$

Expressions for the extrema of the amplitude of the average $\widehat{\overline{D}}(Z_1, Z_2, \alpha^2)$ and relative $\widehat{D}'(Z_1, Z_2, \alpha^2)$ solid displacements are presented in Appendix C.

4.1. Rigid lower surface, $Z_2 \to \pm\infty$

Fig. (2) presents (20) and (22) for the limits of $Z_2 \to \pm\infty$, corresponding to a fixed lower surface $D_2 \sim 0$. Panel (a) presents the magnitude ratio of liquid pressure to external pressure $|P/P_e|$, panel (b) shows the relative phase of liquid pressure $\angle P - \angle P_e$, panel (c) shows the magnitude of deformation normalized by the external pressure $|D_1/P_e|$, and panel (d) shows the relative phase of deformation $\angle D_1 - \angle P_e$.

Panels (a) and (c) in Fig. (2) present maxima of the liquid pressure as well as sheet deformation along a smooth black line defined by

$$\alpha^2 \sim -\frac{5Z_1}{3} \tag{30}$$

(or in dimensional form $\omega^2 \sim 5h_0(s_1k^6 + t_1k^4)/(3\rho_l + 5m_1h_0k^2)$), representing linearization of the extrema condition (29a) with regard to α^2 around $\alpha^2 = 0$ for $|Z_2| \to \infty$.

Fluid inertia thus reduces the resonance frequency of the configuration, which emanates from increasing the mass accelerated during oscillations. On the line $\alpha^2 \sim -5Z_1/3$, the fluidic pressure decreases with α^2, the amplitude of deformation increases with α^2, and the sheet velocity is synchronized with the external pressure $\angle W_1' - \angle P_e = \pi$. Thus for a given deformation amplitude, external oscillating pressure waves apply the maximal external work on the sheet, and thus maximal dissipation, at the line (30). The sheet deformation reaches a global maximum for $\alpha^2 = 0$ and $Z_1 = 0$, corresponding to the resonance frequency of the upper sheet and negligible fluid inertia parallel to the sheets. At the resonance frequency of the upper plate (on the line $Z_1 = 0$), the fluidic Womersley number $\alpha^2 = \rho_l h_0^2\omega/\mu$ does not affect the liquid pressure which is equal to the external pressure in both magnitude and phase. In addition, the liquid pressure amplitude is equal to the external pressure on the line $\alpha^2 \sim -5Z_1/6$, on which however $\angle W_1' - \angle P_e \neq \pi$.

4.2. Equal impedance of the lower and upper sheets, $Z_1 = Z_2$

Fig. 3 shows dynamics for configurations where $Z_1 = Z_2$ (in dimensional terms $-s_1k^4 - t_1k^2 + m_1\omega^2 = -s_2k^4 - t_2k^2 + m_2\omega^2 - s_k$). Panel (a) presents $|P|/|P_e|$, panel (b) shows $\angle P - \angle P_e$, panel (c) shows $|D_1|/|P_e|$, panel (d) shows $\angle D_1 - \angle P_e$, panel (e) shows $|D_2|/|P_e|$, and panel (f) shows $\angle D_2 - \angle P_e$.

For predefined values of α^2 and ratio of sheet impedance $Z_1/Z_2 \equiv R_{12}$, values of Z_1 yielding extrema of fluidic pressure are defined by

$$Z_1 = -\frac{(1+R_{12})F_1(\alpha)}{2F_1^2(\alpha) + 2F_2^2(\alpha)}, \tag{31}$$

which can be approximated by $Z_1 \approx -3(1 + R_{12})\alpha^2/5$ (presented by smooth lines in Fig. 3) in the limit of $\alpha^2 \to 0$. The limit of $(Z_1, Z_2) \to (0, 0)$ yields various values of pressure and displacements depending on the ratio of Z_1/Z_2. For $\lim_{(Z_1,Z_2)\to(0,0)} Z_1/Z_2 = -1$, resonance dynamics are accompanied by significant increase in the magnitude of the fluidic pressure. In contrast, for $\lim_{(Z_1,Z_2)\to(0,0)} Z_1/Z_2 = 1$ the fluidic pressure equals half of the external pressure excitation.

Panel (a) presents the extremum line (31) which is accompanied by a maximum of the relative displacements $|D'|/|P_e|$. This maximum line is similar to the modified resonance of the upper plate presented in Fig. 2a. Panels (c) and (e) present the solid resonances along $Z_1 = Z_2 = Z_1 + Z_2 = 0$ and an additional fluidic maximum of the upper plate near the line (31). Panels (d) and (f) yield a sharp phase difference of D_1 and D_2 between $Z_1 > 0$ and $Z_1 < 0$. Both D_1 and D_2 are near anti-phase for small negative Z_1 and in-phase for small positive Z_1. In contrast, the phase of the fluidic pressure (panel b) presents gradual change near resonance. Panels (a), (c) and (e) show that the resonance of the solid deflection for $Z_1 = Z_2 \to 0$, yields similar oscillations of the upper and lower sheets. These oscillations are accompanied by synchronous liquid pressure with half the magnitude of the external pressure ($|P|/|P_e| = 1/2$ and $\angle P - \angle P_e = 0$). Thus, both sheets are applied with identical excitations at resonance.

4.3. Asymmetric elastic sheets

In Figs. (4) and (5) we examine the effect of modifying the properties of the lower surface on the frequency response and extrema for configurations where $Z_2 = -6, -3, -1$ for the range $-10 \le Z_1 \le 10$ and $0 \le \alpha^2 \le 10$.

Fig. 4 presents scaled fluid pressure amplitude $|P/P_e|$ (left column) and relative phase $\angle P - \angle P_e$ (right column). Panels (a,b) correspond to $Z_2 = -6$, panels (c,d) correspond to $Z_2 = -3$, and panels (e,f) correspond to $Z_2 = -1$. The smooth lines (29a) represent values of Z_1 yielding extrema of the liquid pressure amplitude for set values of (α^2, Z_2). The dotted lines (29c) present, similarly, values of α^2 for set values of (Z_1, Z_2).

For $Z_2 = -6$, panel (a) presents maxima and saddle points along (29c) where the maximum associated with $\alpha^2 = 0$ is on $Z_1 = -(1/Z_2 + 4Z_2/9)^{-1}$, not on $Z_1 = 0$. In this case the fluid inertia decreases the resonance frequency, similarly to the cases presented in Figs. 2 and 3. However, as Z_2 increases additional maximum emerge (see panel c) and coalesce (see panel e) to a single line near $Z_1 \approx -(1/Z_2 + 4Z_2/9)^{-1}$ in which the magnitude of the derivative of fluid pressure amplitude and phase with regard to Z_1 sharply increases. This new extremum emanates from a combined fluid-elastic interaction increasing the fluidic pressure (see Eq. (22)) and not a modified solid resonance. As Z_2 becomes smaller, configurations with positive values of Z_1

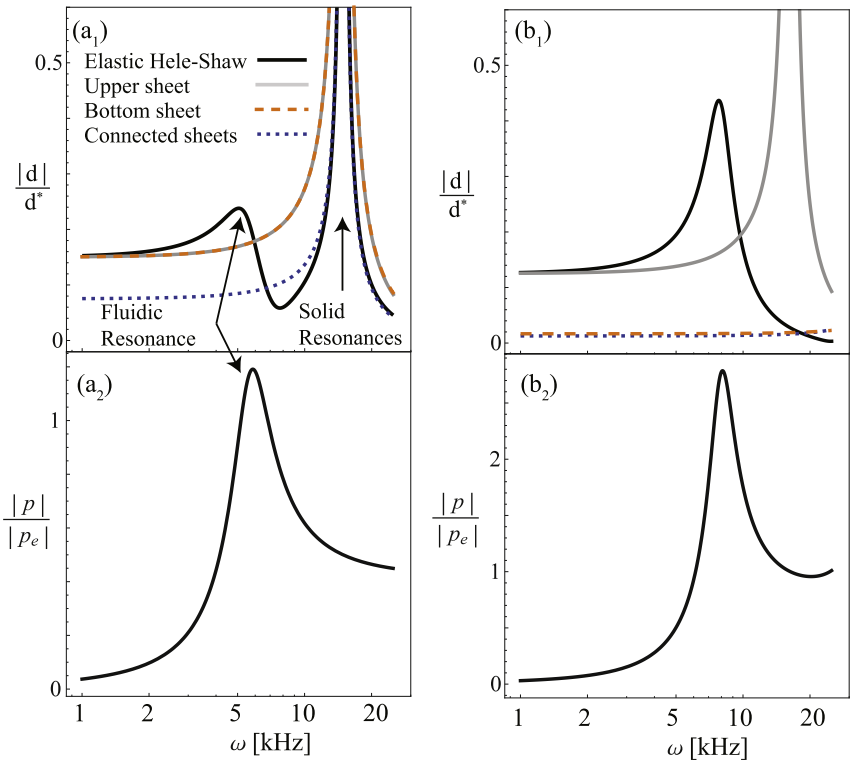

Fig. 6. Illustration of the additional resonance frequency emerging due to parallel motion of fluid. Panels (a_1, a_2) examine equal sheet impedance $Z_1 = Z_2$. Normalized displacement of the upper sheet (a_1, b_1) and fluidic pressure (a_2, b_2) for an elastic Hele-Shaw are marked by smooth black lines. For comparison, the isolated solid response of the upper sheet (grey lines), the bottom sheet (dashed orange lines) and the two sheets with a constraint of constant gap (blue dashed) are presented. (For interpretation of the references to color in this figure legend, the reader is referred to the Web version of this article.)

become increasingly synchronized with the external pressure and the liquid pressure, whereas configurations with negative Z_1 approach the inverse phase of $-180°$. The fluidic pressure amplitude is equal to the external amplitude on two curves, one of which is the upper sheet resonance frequencies line $Z_1 = 0$.

Fig. 5 focuses on elastic deflection and presents the magnitude of average deformation $|\overline{D}|/|P_e|$ (left column), and the relative deformation $|D'|/|P_e|$ (right column) as a function of α^2 and Z_1 for identical parameter range as in Fig. 4. The smooth and dotted lines represent extremum of deflection with regard to Z_1 (for set values of α^2, Z_2) and with regard to α^2 (for set values of Z_1, Z_2), respectively, see Appendix C. The patterns presented for both the scaled average deflection $|\overline{D}|/|P_e|$ and scaled relative deflection $|D'|/|P_e|$ closely follow that of the fluidic pressure. The average deflection $|\overline{D}|/|P_e|$ does not involve viscous flow and is thus undamped, in contrast with $|D'|/|P_e|$. Hence, while far from resonance the magnitude of $|\overline{D}|/|P_e|$ and $|D'|/|P_e|$ are similar, near resonance frequencies (e.g. near the line $Z_1 \approx -(1/Z_2 + 4Z_2/9)^{-1}$ for $Z_2 = -1$), the ratio $|\overline{D}|/|D'|$ increases indefinitely and eventually invalidates the model assumption of $O(|\overline{D}|) \sim O(|D'|)$.

5. Discussion

In Section 4 the response of an elastic Hele-Shaw cell was presented in terms of the parameters (α, Z_1, Z_2), which combine effects of elasticity, viscosity, fluid and solid inertia, as well as the frequency and wavelength of the excitation. While Figs. 2–5 describe a wide range of parameters, the effect of changing excitation frequency or wavelength of a specific configuration requires following curved lines (e.g. on $Z_n = (-s_n k^4 - t_n k^2 + m_n \omega^2 - s_k(n-1))/(\mu\omega/h_0^3 k^2)$, $n = 1, 2$ in Figs. 2 and 3) or interpolation between panels (as in Figs. 4 and 5). Clarity might thus benefit from a less general but explicit presentation of the amplitude of the fluidic pressure and elastic displacement vs. the excitation frequency for specific and constant physical parameters. In addition, the effect of the fluid will be emphasized here by comparison with relevant fully elastic configurations.

5.1. The emergence of an additional fluid-elastic resonance frequency

In the limit of negligible fluidic effects the dynamics of the upper surface will approach the dynamics of an isolated sheet. Alternatively, in the limit of a highly viscous fluid the configuration will be similar to two elastic sheets with a constraint of constant gap (see Appendix D). Thus, we expect multiple elastic resonance frequencies defined by $Z_1 = 0, Z_2 = 0$ and $Z_1 + Z_2 = 0$

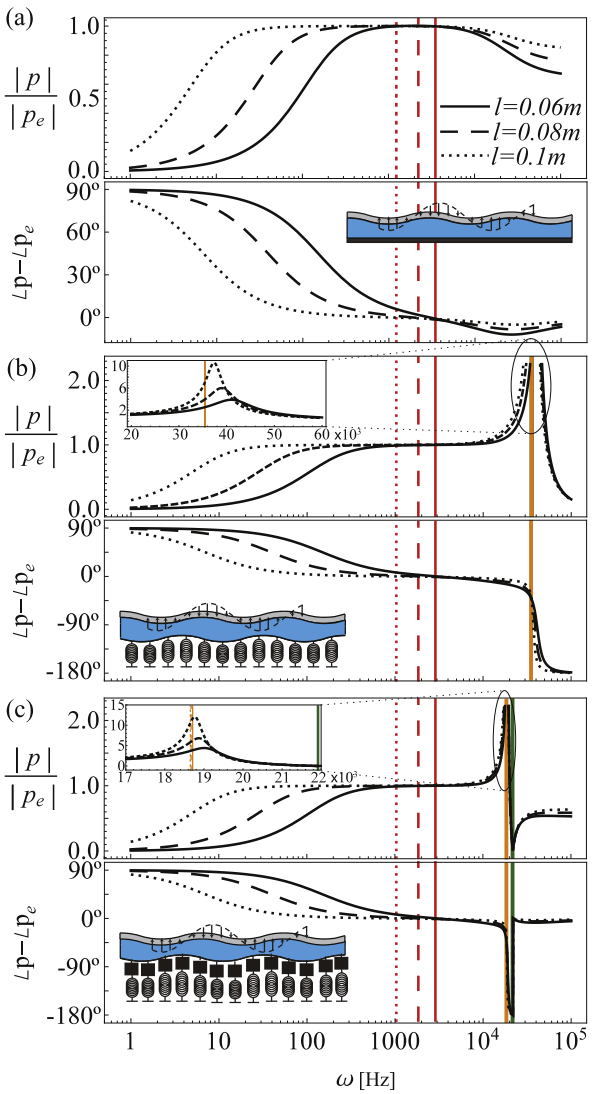

Fig. 7. Frequency response of elastic Hele-Shaw cells for three physical configurations. In panel (a) the bottom surface is rigid. In panel (b) the bottom surface is mass-less and compliant. In panel (c) the bottom surface mass is finite and compliant. Red, green, and orange vertical lines correspond to resonance frequencies of the upper sheet, the lower substrate, and a combine reference configuration with a constraint of constant gap between the upper sheet and the lower surface. (For interpretation of the references to color in this figure legend, the reader is referred to the Web version of this article.)

to appear. However, from Figs. 2–5 an additional response frequency is evident, which involves the interaction between motion of fluid parallel to the elastic sheets and elastic displacements and external actuation perpendicular to the sheets.

This fluid-elastic resonance is presented in Fig. 6 for two illustrative configurations. Panel (a) examines the normalized displacement of the upper sheet (a_1) and fluid pressure amplitude (a_2) of identical sheets $Z_1 = Z_2$ (defined by $\rho_1 = \rho_2 = 10^3 \mathrm{Kg/m^3}$, $s_1 = s_2 = 0.054\,\mathrm{Pa/m^3}$, $m_1 = m_2 = 1\,\mathrm{Kg/m^2}$, $\mu = 1\,\mathrm{Pa}\cdot s$, $\rho_l = 10^3 \mathrm{Kg/m^3}$, $h_0 = 10^{-3}\mathrm{m}$, $2b_1 = 2b_2 = 0.001\,\mathrm{m}, k = 450\,\mathrm{m^{-1}}, t_1 = t_2 = s_k = 0$). Panel (b) similarly presents upper sheet normalized displacement (b_1) and fluid pressure amplitude (b_2) for configuration where $Z_2 \gg Z_1$, (defined by $\rho_1 = \rho_2 = 10^3 \mathrm{Kg/m^3}$, $s_1 = 0.0065\,\mathrm{Pa/m^3}$, $s_2 = 0.057\,\mathrm{Pa/m^3}$, $m_1 = m_2 = 1\,\mathrm{Kg/m^2}$, $\mu = 1\,\mathrm{Pa}\cdot s$, $\rho_l = 10^3 \mathrm{Kg/m^3}$, $h_0 = 10^{-3}$, $2b_1 = 2b_2 = 10^{-3}\mathrm{m}$, $k = 450\,\mathrm{m^{-1}}$, $t_1 = t_2 = s_k = 0$). Normalized deformation magnitude of the upper plate of elastic Hele-Shaw cell is marked by black smooth lines. Grey, dashed-orange and dotted-blue lines mark relevant fully elastic configurations of the upper sheet, lower sheet and connected elastic sheets, respectively. All deformations are scaled by $d^* = 3 \cdot 10^{-6}\mathrm{m}$.

For both configurations presented in panels (a) and (b), at lower frequencies corresponding to $|Z_1| \gg 1$, the amplitude of fluid pressure decreases with ω and displacement of the top sheet is identical to that of an isolated elastic sheet. For the opposite limit of large ω, corresponding to $|Z_1|, |Z_2| \ll 1$, the elastic Hele-Shaw cell oscillates as two elastic sheets with a constraint of constant gap (see Appendix D). For panel (a), in accordance with the results presented in Fig. 3, the identical properties of the bottom and top sheets yield a single solid resonance frequency $\omega \approx 14.9\,\mathrm{KHz}$ accompanied by $|p/p_e| = 0.5$. In addition to

this elastic resonance frequency, a clear additional extremum frequency is evident at $\omega \approx 5.05$ KHz, near the extremum of the fluidic pressure at $\omega \approx 5.05$ KHz. A similar deformation extremum is presented in panel (b) for $\omega \approx 7.77$ KHz, near the pressure extremum of $\omega \approx 8.09$ KHz, in which it is the dominant resonance frequency due to the rigid lower elastic sheet eliminating other solid resonances.

5.2. Elastic Hele-Shaw cell as a mechanical filter

A mechanical filter is a device designed to amplify or reduce external excitation based on frequency. It is common to describe such devices by an analogue to electrical filters. Examining an elastic Hele-Shaw cell as a mechanical filter, the effects of elasticity, inertia and viscosity are analogues to electrical components of capacitance, inductance and resistance. Similarly to the analysis of electric filters, we are interested in characterizing the mechanical impedance of an Elastic Hele-Shaw cell.

Fig. 7 presents the magnitude and phase of liquid pressure vs. excitation frequency ω for wavelengths of $l = 0.06, 0.08$ and 0.1 m, denoted by the solid, dashed, and dotted lines, respectively. Vertical lines denote resonance frequency of the reference solid configurations of the upper sheet (red), bottom surface (green) and two sheets with a constraint of constant gap (orange). In all panels (a-c) the properties of the upper sheet and fluid layer are defined by bending resistance $s_1 = 0.8\,\mathrm{Pa\,m^3}$, sheet thickness $b_1 = 1$ cm, sheet density $\rho_1 = 954\,\mathrm{Kg/m^3}$, liquid viscosity $\mu = 60\,\mathrm{Pa}\cdot s$, liquid gap height $2h_0 = 5$ mm, and liquid density $\rho_l = 750\,\mathrm{Kg/m^2}$ (characteristic to rubber and silicon oil). In panel (a) the bottom surface is rigid. In panel (b) the bottom surface is an elastic spring array with $s_k = 12\,\mathrm{GPa/m}$. In panel (c) the bottom surface is an elastic spring array with $s_k = 12\,\mathrm{GPa/m}$ and mass-per-area of $m_2 = 25\,\mathrm{Kg/m^2}$.

In all of the configurations, sufficiently small frequencies yield negligible liquid pressure amplitude. An intermediate range of frequencies, which include the resonance frequency of the elastic sheet, leads to liquid pressure with amplitude and phase identical to the external pressure. In configuration (a) large frequencies lead to decay of the liquid pressure due to growing dominance of the elastic sheet inertia. Thus, for $Z_2 \to \pm\infty$, the response of the system is similar to a bandpass filter and the fluidic pressure cannot exceed the external excitation. In configuration (b), similar behaviour is observed with an additional peak of the fluidic pressure near the elastic resonance frequency defined by (29a)-(29c) (at $\omega \approx 40$ KHz). At greater frequencies both the liquid pressure and phase decay to zero. Configuration (c) involves an additional resonance frequency of the lower surface, yielding a minima of the pressure near the combined reference resonance ($Z_1 + Z_2 = 0$).

6. Concluding remarks

This work theoretically examined the frequency response of two parallel elastic sheets containing a thin liquid film, excited by traveling pressure waves. Applying the linearized plate model for the elastic sheets, order-of-magnitude analysis yielded that fluidic non-linear inertial terms are negligible compared with the linear terms, allowing the linearization of the Navier-Stokes equations. Phase and amplitude of traveling-wave solutions were calculated by modal analysis and were utilized to present a comprehensive parametric study of frequency response in terms of solid displacements and fluidic pressure for various configurations. The results presented a new resonance frequency related to fluid acceleration parallel to the sheets, as well as a bandpass filter behaviour of such configurations.

The presented analysis focused on configurations where the average and relative displacements are of similar order of magnitude $O(\widehat{D}') \sim O(\widehat{\overline{D}})$. In the limit of $\widehat{D}' \ll \widehat{\overline{D}}$ (presented in Appendix A), although liquid pressure is created by elastic displacements, it is not significant in determining the displacement dynamics. While the modal analysis examined response to wave excitation with a single frequency and amplitude, the three-dimensional response dynamics for an arbitrary external pressure field is immediately obtained from an inverse Fourier transform (see Appendix B).

While the presented results clearly showed that a viscous layer may be used to improve the system mechanical response to external excitation, further study is required in order to practically realize such protective layers. Specifically of interest is examining effects of a localized sudden load as well as effect of boundary conditions on the mechanical impedance. Viscous-elastic dynamics can also be introduced to other commonly used protective layers such as honeycomb structures which include interconnected fluid-filled pores, and periodically laminated structures containing multiple viscous layers.

Appendix A. Leading order equations for $d'^*/\overline{d}^* \ll 1$

For dynamics characterized by $d'^*/\overline{d}^* \sim \varepsilon_1^2 \ll 1$ order of magnitude yields that the convection terms $\rho(\boldsymbol{u}_\parallel, w)\cdot\left(\boldsymbol{\nabla}_\parallel, \partial/\partial z\right)(\boldsymbol{u}_\parallel, w)$ in Eq. (2) scales as R_e/ε_1 and may not be neglected. In addition, the sheets mean acceleration $\partial\overline{d}^2/\partial t^2$ yields significant pressures gradients in the transverse direction ($\partial p/\partial z$). Thus, the leading order governing Eq. (12) are of the form

$$\alpha^2\frac{\partial \boldsymbol{U}}{\partial T} + \frac{\mathrm{Re}}{\varepsilon_1}\frac{\partial \overline{D}}{\partial T}\frac{\partial \boldsymbol{U}}{\partial Z} = -\boldsymbol{\nabla}P + \frac{\partial^2 \boldsymbol{U}}{\partial Z^2} + O(\varepsilon_1^2, \varepsilon_1\mathrm{Re},), \tag{A.1a}$$

$$\alpha^2\frac{\partial^2 \overline{D}}{\partial T^2} = -\frac{\partial P}{\partial Z} + O\left(\varepsilon_1^2, \varepsilon_1\mathrm{Re}\right), \tag{A.1b}$$

$$\frac{\partial W'}{\partial Z} + \boldsymbol{\nabla}\cdot\boldsymbol{U} = 0, \tag{A.1c}$$

and leading order boundary conditions (13) are

$$W'(Z=1) + W'(Z=-1) = O(\varepsilon_2), \tag{A.2a}$$

$$W'(Z=1) - W'(Z=-1) = 2\frac{\partial D'}{\partial T} + O(\varepsilon_2), \tag{A.2b}$$

$$\boldsymbol{U}(Z=1) = O(b_1 k\varepsilon_1), \quad \boldsymbol{U}(Z=-1) \sim O(b_2 k\varepsilon_1), \tag{A.2c}$$

$$\left[\left(-s_1 k^4\nabla^4 + t_1 k^2\nabla^2 - m_1\omega^2\frac{\partial^2}{\partial T^2}\right)\frac{h_0}{\mu\omega}\right](\overline{D} + \varepsilon_1^2 D') + P - P_e = 0, \tag{A.2d}$$

$$\left[\left(-s_2 k^4\nabla^4 + t_2 k^2\nabla^2 - s_k - m_2\omega^2\frac{\partial^2}{\partial T^2}\right)\frac{h_0}{\mu\omega}\right](\overline{D} - \varepsilon_1^2 D') - P = 0. \tag{A.2e}$$

Eqs. (A.1) and (A.2) yield that in the leading order dynamics for $d'^*/\overline{d}^* \sim \varepsilon_1^2 \ll 1$, the liquid pressure is created by elastic displacements, but is not significant in determining displacement dynamics of steady-state solutions.

Appendix B. Results in dimensional form

We present here the steady-state oscillating solutions in dimensional form. The dimensional liquid pressure (22) is

$$\widehat{p} = \left(\begin{array}{r} \dfrac{2h_0 k^2(-s_1 k^4 - t_1 k^2 + m_1\omega^2)}{\rho_l\omega^2}\left(1 - \dfrac{\tanh(\sqrt{\rho_l h_0^2\omega i/\mu})}{\sqrt{\rho_l h_0^2\omega i/\mu}}\right) \\ +1 + \dfrac{-s_1 k^4 - t_1 k^2 + m_1\omega^2}{-s_2 k^4 - t_2 k^2 - s_k + m_2\omega^2} \end{array}\right)^{-1} \widehat{p}_e, \tag{B.1}$$

the dimensional longitudinal (18) and transverse (19) liquid velocities are

$$\widehat{u} = \left(\frac{\cosh(\sqrt{\rho_l\omega i/\mu}z)}{\cosh(\sqrt{\rho_l\omega i/\mu}h_0)} - 1\right)\frac{k\widehat{p}}{\omega\rho_l} \tag{B.2}$$

and

$$\widehat{w}' = i\left(\frac{z}{h_0} - \frac{\sinh(\sqrt{\rho_l\omega i/\mu}z)}{\sqrt{\rho_l\omega i/\mu}h_0\cosh(\sqrt{\rho_l\omega i/\mu}h_0)}\right)\frac{k^2 h_0\widehat{p}}{\omega\rho_l}. \tag{B.3}$$

The dimensional relative deformation (20) is

$$\widehat{d}' = \left(1 - \frac{\tanh(\sqrt{\rho_l\omega i/\mu}h_0)}{\sqrt{\rho_l\omega i/\mu}h_0}\right)\frac{k^2 h_0\widehat{p}}{\omega^2\rho_l} \tag{B.4}$$

and the dimensional mean sheet deformation (21) is

$$\overline{d} = \left(1 - \frac{\tanh(\sqrt{\rho_l\omega i/\mu}h_0)}{\sqrt{\rho_l\omega i/\mu}h_0} + \frac{\mu\omega}{h_0^3 k^2(-s_2 k^4 - t_2 k^2 - s_k + m_2\omega^2)}\right)\frac{h_0 k^2\widehat{p}}{\rho_l\omega^2} \tag{B.5}$$

The three-dimensional response dynamics for an arbitrary external pressure field is therefore given in dimensional form by Ref. [30].

$$\begin{pmatrix} p \\ u_x \\ v_y \\ w' \\ \overline{d} \\ d' \end{pmatrix} = \frac{1}{(2\pi)^{3/2}}\int_{-\infty}^{\infty}\int_{-\infty}^{\infty}\int_{-\infty}^{\infty}\widehat{\begin{pmatrix} \widehat{p} \\ k_x\widehat{u}/k \\ k_y\widehat{u}/k \\ \widehat{w}' \\ \widehat{\overline{d}} \\ \widehat{d}' \end{pmatrix}} e^{-i(k_x x + k_y y + \omega t)}dk_x dk_y d\omega, \tag{B.6}$$

where $\sqrt{k_x^2+k_y^2}=k$, and u_x, u_y denote the x, y direction velocity components and $\widehat{p}_e$ is calculated from the inverse transformation

$$\widehat{p}_e(k_x,k_y,\omega)=\frac{1}{(2\pi)^{3/2}}\int_{-\infty}^{\infty}\int_{-\infty}^{\infty}\int_{-\infty}^{\infty}p_e(x,y,t)e^{i(k_x x+k_y y+\omega t)}dxdydt. \tag{B.7}$$

Eqs. (B.6) and (B.7) require the dimensional form since the normalization of the two-dimensional problem was dependent on k and ω.

Appendix C. Extrema points of $\widehat{D}'(Z_1,Z_2,\alpha^2)$, $\widehat{\widetilde{D}}(Z_1,Z_2,\alpha^2)$

We obtain extrema points of the magnitude of $\widehat{D}'=F\widehat{P}$. The solution consists of the liquid pressure multiplied by $F=F_1+iF_2=(\alpha^2)^{-1}(1-\tanh(\sqrt{\alpha^2 i})/\sqrt{\alpha^2 i})$. Thus, extrema points with respect to Z_1, Z_2 (where the remaining variables are kept constant) will yield the same expressions as for the liquid pressure - Eq. (29a) and (29b), respectively. We now obtain extremum points with respect to α^2. We simplify the problem by investigating

$$\left|\frac{\widehat{P}_e}{\widehat{D}'}\right|^2=\frac{(2Z_1F_1+1+Z_1Z_2^{-1})^2+(2Z_1F_2)^2}{F_1^2+F_2^2}. \tag{C.1}$$

Differentiating with respect to α^2 and equating to zero yields

$$Z_1\left(4\frac{\partial F_1}{\partial\alpha^2}|F|^2-(4F_1+Z_2^{-1})\frac{\partial|F|^2}{\partial\alpha^2}\right)-\frac{\partial|F|^2}{\partial\alpha^2}=0. \tag{C.2}$$

We now obtain extremum points of the magnitude of $\widehat{\widetilde{D}}=(F+Z_2^{-1})\widehat{P}$. The equation defining the extremum point of $\widehat{\widetilde{D}}$ with respect to Z_1 is the same as the liquid pressure and relative deformation and is defined by (29a). Next we obtain an expression for the extrema point of $\widehat{\widetilde{D}}$ for α^2. We simplify the problem by investigating

$$\left|\frac{\widehat{P}_e}{\widehat{\widetilde{D}}}\right|^2=\frac{(2Z_1F_1+1+Z_1Z_2^{-1})^2+(2Z_1F_2)^2}{(F_1+Z_2^{-1})^2+F_2^2}. \tag{C.3}$$

By differentiating (C.3) with respect to α^2 and equating to zero yields an inexplicit relationship

$$AZ_1^2+BZ_1+C=0, \tag{C.4}$$

where $A=\partial_{\alpha^2}((2F_1+Z_2^{-1})^2+(2F_2)^2)\times((F_1+Z_2^{-1})^2+F_2^2)^{-1}$, $B=\partial_{\alpha^2}(4F_1+Z_2^{-1})\times((F_1+Z_2^{-1})^2+F_2^2)^{-1}$, and $C=\partial_{\alpha^2}((F_1+Z_2^{-1})^2+F_2^2)^{-1}$. We may solve (C.4) as a quadratic equation in terms of Z_1 and obtain a functional relationship between Z_1 to Z_2 and α^2.

Appendix D. Comparison between dynamics of two sheets connected by a stiff spring array to an elastic Hele-Shaw cell

We here calculate the phase and amplitude of the steady state oscillations for a reference configuration consisting of two elastic sheets connected by a spring array with coefficient s_{12}. The response of two elastic sheets with a constraint of constant gap or an isolated upper sheet is obtained directly from limits of the spring array coefficient.

The governing equation of the upper elastic sheet is

$$-s_1\frac{\partial^4 d_1}{\partial x^4}+t_1\frac{\partial^2 d_1}{\partial x^2}-s_{12}(d_1-d_2)-p_e=m_1\frac{\partial^2 d_1}{\partial t^2}, \tag{D.1}$$

and the governing equation of the lower elastic sheet is

$$-s_2\frac{\partial^4 d_2}{\partial x^4}+t_2\frac{\partial^2 d_2}{\partial x^2}-s_k d_2+s_{12}(d_1-d_2)=m_2\frac{\partial^2 d_2}{\partial t^2}, \tag{D.2}$$

where s_{12} is the spring stiffness connecting the sheets. We substitute the wave form

$$f=\widehat{f}e^{i(kx+\omega t)},\quad f=d_1,d_2,p_e, \tag{D.3}$$

for all variables, and obtain the upper sheet deformation

$$\widehat{d}_1=\frac{\widetilde{z}_2-s_{12}}{(\widetilde{z}_2-s_{12})(\widetilde{z}_1-s_{12})-s_{12}^2}\widehat{p}_e, \tag{D.4}$$

and the lower sheet deformation

$$\widehat{d}_2=\frac{-s_{12}}{(\widetilde{z}_2-s_{12})(\widetilde{z}_1-s_{12})-s_{12}^2}\widehat{p}_e. \tag{D.5}$$

where $\widetilde{z}_n = -s_n k^4 - t_n k^2 + m_n \omega^2 - s_k(n-1), \quad n = 1, 2$. From Eq. (D.5), and (D.4) we see that resonance is obtained when

$$(\widetilde{z}_2 - s_{12})(\widetilde{z}_1 - s_{12}) - s_{12}^2 = 0 \tag{D.6}$$

isolating $\widetilde{z}_1$ we obtain

$$\widetilde{z}_1 = \left(\frac{1}{s_{12}} - \frac{1}{\widetilde{z}_2}\right)^{-1} \tag{D.7}$$

for the case the spring is much stiffer than the sheets we obtain that resonance will occur at $\widetilde{z}_1 = -\widetilde{z}_2$. The case of which the spring is much softer than z_1 yields an isolated upper sheet.

Appendix E. Supplementary data

Supplementary data related to this article can be found at https://doi.org/10.1016/j.jsv.2018.08.047.

References

[1] A. Hosoi, L. Mahadevan, Peeling, healing, and bursting in a lubricated elastic sheet, Phys. Rev. Lett. 93 (13) (2004) 137802.
[2] J. Lister, G. Peng, J. Neufeld, Viscous control of peeling an elastic sheet by bending and pulling, Phys. Rev. Lett. 111 (15) (2013) 154501.
[3] G.G. Peng, D. Pihler-Puzović, A. Juel, M. Heil, J.R. Lister, Displacement flows under elastic membranes. part 2. analysis of interfacial effects, J. Fluid Mech. 784 (2015) 512–547.
[4] D. Pihler-Puzović, A. Juel, G.G. Peng, J.R. Lister, M. Heil, Displacement flows under elastic membranes. Part 1. Experiments and direct numerical simulations, J. Fluid Mech. 784 (2015) 487–511.
[5] A. Carlson, L. Mahadevan, Similarity and singularity in adhesive elastohydrodynamic touchdown, Phys. Fluids 28 (1) (2016) 011702 (1994-present).
[6] S. Roper, J. Lister, Buoyancy-driven crack propagation from an over-pressured source, J. Fluid Mech. 536 (2005) 79–98.
[7] D. Spence, P. Sharp, D. Turcotte, Buoyancy-driven crack propagation: a mechanism for magma migration, J. Fluid Mech. 174 (1987) 135–153.
[8] C.-Y. Lai, Z. Zheng, E. Dressaire, G.Z. Ramon, H.E. Huppert, H.A. Stone, Elastic relaxation of fluid-driven cracks and the resulting backflow, Phys. Rev. Lett. 117 (26) (2016) 268001.
[9] I. Hewitt, N. Balmforth, J. De Bruyn, Elastic-plated gravity currents, Eur. J. Appl. Math. 26 (1) (2015) 1–31.
[10] P. Howell, H. Kim, M. Popova, H. Stone, Rivulet flow over a flexible beam, J. Fluid Mech. 796 (2016) 285–305.
[11] R. Huang, Z. Suo, Wrinkling of a compressed elastic film on a viscous layer, J. Appl. Phys. 91 (3) (2002) 1135–1142.
[12] O. Kodio, I.M. Griffiths, D. Vella, Lubricated wrinkles: imposed constraints affect the dynamics of wrinkle coarsening, Phys. Rev. Fluids 2 (1) (2017) 014202.
[13] H. Lamb, On the vibrations of an elastic plate in contact with water, Proc. R. Soc. Lond. - Ser. A Contain. Pap. A Math. Phys. Charact. 98 (690) (1920) 205–216.
[14] N. McLachlan, The accession to inertia of flexible discs vibrating in a fluid, Proc. Phys. Soc. 44 (5) (1932) 546.
[15] W.H. Peake, E.G. Thurston, The lowest resonant frequency of a water-loaded circular plate, J. Acoust. Soc. Am. 26 (2) (1954) 166–168.
[16] F.M. De Espinosa, J. Gallego-Juarez, On the resonance frequencies of water-loaded circular plates, J. Sound Vib. 94 (2) (1984) 217–222.
[17] D. Crighton, J. Oswell, Fluid loading with mean flow. i. response of an elastic plate to localized excitation, Phil. Trans. Roy. Soc. Lond. Math., Phys. Eng. Sci. 335 (1639) (1991) 557–592.
[18] N. Peake, S. Sorokin, On the behaviour of fluid-loaded sandwich panels with mean flow, J. Sound Vib. 242 (4) (2001) 597–617.
[19] S. Sorokin, Analysis of vibrations and energy flows in sandwich plates bearing concentrated masses and spring-like inclusions in heavy fluid-loading conditions, J. Sound Vib. 253 (2) (2002) 485–505.
[20] C. Chang, C. Hsu, Control performance of liquid column vibration absorbers, Eng. Struct. 20 (7) (1998) 580–586.
[21] X. Zeng, Y. Yu, L. Zhang, Q. Liu, H. Wu, A new energy-absorbing device for motion suppression in deep-sea floating platforms, Energies 8 (1) (2014) 111–132.
[22] M. Symans, M. Constantinou, Passive fluid viscous damping systems for seismic energy dissipation, ISET J. Earthq. Technol. 35 (4) (1998) 185–206.
[23] C. Hou, Fluid dynamics and behavior of nonlinear viscous fluid dampers, J. Struct. Eng. 134 (1) (2008) 56–63.
[24] H. Laun, R. Bung, F. Schmidt, Rheology of extremely shear thickening polymer dispersionsa)(passively viscosity switching fluids), J. Rheol. 35 (6) (1991) 999–1034.
[25] N. Wagner, E. Wetzel, Advanced Body Armor Utilizing Shear Thickening Fluids, 2002.
[26] C. Fischer, S. Braun, P. Bourban, V. Michaud, C. Plummer, J. Månson, Dynamic properties of sandwich structures with integrated shear-thickening fluids, Smart Mater. Struct. 15 (5) (2006) 1467.
[27] C. Suciu, T. Iwatsubo, S. Deki, Investigation of a colloidal damper, J. Colloid Interface Sci. 259 (1) (2003) 62–80.
[28] A. Tulchinsky, A.D. Gat, Transient dynamics of an elastic hele-shaw cell due to external forces with application to impact mitigation, J. Fluid Mech. 800 (2016) 517–530.
[29] P. Howell, G. Kozyreff, J. Ockendon, Applied Solid Mechanics, Cambridge University Press, 2009. no. 43.
[30] G.B. Arfken, H.J. Weber, F.E. Harris, Mathematical Methods for Physicists: a Comprehensive Guide, Academic press, 2011.